Insertion Loss and Crosstalk Analysis of a Fiber Switch Based on a Pixelized Phase Modulator

David Sinefeld and Dan M. Marom, *Senior Member, IEEE*

***Abstract*—We analyze the performance of a spatial fiber switching system when using a pixelized mirror, such as a LCoS or MEMS spatial light modulator, in place of a large tilting micromirror. Our findings demonstrate the dependence of insertion losses on tilt angles or fiber counts, and the dependence of the crosstalk in the number of phase quantization levels and random phase errors. The former effects can be minimized by satisfying a relationship between the tilt angle to a fiber, the pitch of the array, and the optical wavelength.**

***Index Terms*—Microelectromechanical devices, multiplexers, optical fiber communication, optical switches, spatial light modulators (SLMs).**

I. Introduction

OPTICAL switching between a single input fiber and multiple output fibers is often implemented with a free-space arrangement using a single tilting mirror that performs the task of beam steering [1] [see Fig. 1(Top)]. A diffraction grating may be inserted into the optical path to construct a wavelength-selective switch version [2] [see Fig. 1(Bottom)], in which case a 1-D array of tilting micromirrors is required, one for every wavelength channel. Both the single tilting mirror and the micromirror array are usually implemented using microelectromechanical system (MEMS) technology, which is based on processing of silicon to construct moving structures. However, some system vendors are averse to using MEMS tilting micromirrors in telecom components and subsystems, due to concerns of stability, repeatability, fatigue, and aging. While it has been shown that by proper design such concerns can be laid to rest [3], there is still intense interest in alternative beam-steering solutions [4].

Recent technological advances in large, 2-D array, spatial light modulators (SLMs)—which were originally developed for high-resolution image projection application—can also be utilized for beam steering. The SLM has to be configured to modulate phase instead of amplitude, and beam steering is achieved by prescribing a linear phase ramp. Modern SLM panels are often based on a liquid--crystal on silicon (LCoS) device, which utilizes a silicon chip for defining and electrically addressing the individual pixels of the array, with no moving parts [5]. MEMS-based panels are also available, where pixel modulation is achieved with piston motion pixels [6].

Manuscript received July 04, 2010; revised September 08, 2010; accepted October 25, 2010. Date of publication November 11, 2010; date of current version January 05, 2011. This work was supported in part by the Israel Science Foundation under Grant 1359/07 and in part by The Peter Brojde Center for Innovative Engineering.

The authors are with the Applied Physics Department, The Hebrew University of Jerusalem, Jerusalem 91904, Israel (e-mail: sinefeld@gmail.com; danmarom@cc.huji.ac.il).

Color versions of one or more of the figures in this paper are available online at http://ieeexplore.ieee.org

Digital Object Identifier 10.1109/JLT.2010.2091623

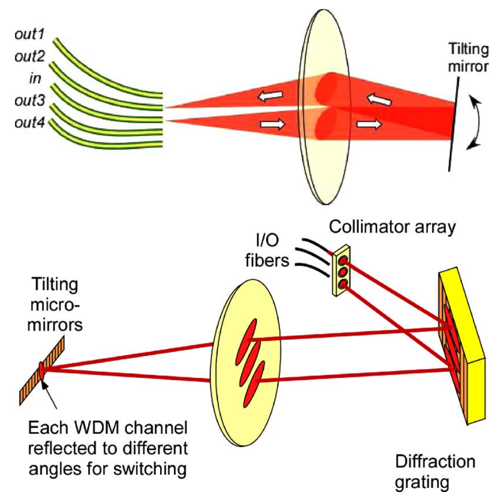

Fig. 1. Switches based on beam-steering architecture. Top: Switching from an input fiber to any output fiber, as determined by the mirror tilt angle. Bottom: Fiber switching on a wavelength-basis, as determined by the mirror tilt angle in the mirror array, where each mirror is assigned for each wavelength.

In this paper, we offer a rigorous analysis of the performance associated with beam scanning switches, when the mirror is implemented with a phase SLM instead of a tilting mirror. We analytically calculate the fiber coupling integral to the desired fiber to which the optical signal is routed, as well as to the other fibers giving rise to crosstalk. We take into account the effects of pixel size and phase level quantization. We find that the insertion loss to the desired fiber increases as the number of pixels spanning the full 2π phase period decreases. Additionally, we find that the crosstalk to the other fibers increases as the number of discrete phase levels that can be prescribed decreases. A statistical analysis of random phase errors was also performed, showing the impact of phase errors on the crosstalk. Hence, the ideal SLM should have infinitesimally-small pixels and continuous, as opposed to discrete, gray level representation, hence approaching the performance of a bulk tilting mirror.

Due to the generality of the discussion, we avoid including effects that are typical to a specific SLM type. LCOS SLM suffer mostly from the fringe-field effect between pixels [7] , whereas MEMS modulators have a lower fill factor, which reduces the diffraction efficiency; both effects were omitted from our analysis.

The paper is structured as follows: in Section II, we describe the system model and our method of calculation, in Section III, the performance (e.g., fiber coupling and crosstalk) of a simple system with a continuous mirror as the phase deflector is discussed, in Section IV, the mirror is replaced with a phase SLM where the pixelization effect is being taken into account. Finally in Section V, the addition of random

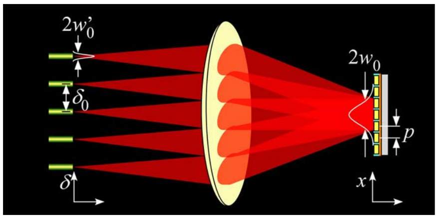

Fig. 2. Schematic of pixelized switch: A Fourier lens disposed between fiber plane and pixelated SLM plane is collimating the light from the fiber on a pixelized SLM with pixel size p. w_0' is the beam waist at the end of the fiber, and w_0 is the beam waist at the SLM plane. The fibers are aligned in a row along the δ axis with the input fiber at the center.

phase noise is discussed where we calculate both the average and standard deviation of the power coupling integral.

II. System Analysis Model

Our analytic calculations are based on the optical switching system, as shown in Fig. 2. An input signal, coming from the central fiber is collimated by a Fourier lens (with a focal length f) onto a pixelized SLM plane. A linear phase ramp is then added to the beam in order to deflect the light to the chosen output fiber. Our calculations were made for a 1-D 1 $\times$ 10 fiber switch, where all the fiber ports are aligned in a row along the δ axis, with the input fiber at the center. The reflected beam can be directed upwardsor downward to outer fiber positions, using beam steering to select the desired output fiber. The fiber ports are separated by distance δ_0 , which satisfies a 40 dB isolation criterion between fibers as will be shown in detail in the following.

All the beams coming from the fiber ports are modeled as Gaussian, which provides satisfactory fiber coupling results, whether the output port is coming directly from the fiber end or from a collimator. In order to simplify the calculations, the analysis was done by solving the fiber coupling integral at the device (Fourier) plane in one dimension only.

Starting with w_0' as the Gaussian beam radius at the center fiber output, the spot size on the phase SLM (which is Gaussian as well) is given by $w_0 = \lambda f/\pi w_0'$. The Gaussian field distribution on the SLM plane is therefore:

$$\psi_{\rm in}(x) = \left(\frac{2}{\pi w_0^2}\right)^{1/4} \exp\left[-\frac{x^2}{w_0^2}\right] = \left(\frac{2\pi w_0'^2}{\lambda^2 f^2}\right)^{1/4} \exp\left[-\frac{w_0'^2 x^2}{(\lambda f/\pi)^2}\right] \tag{1}$$

where λ is the wavelength, f is the Fourier lens focal length, and x is the spatial coordinate along the SLM plane. The field in (1) is normalized such that the coupling integral is unity

$$\int \psi_{\rm in}(x)\psi_{\rm in}^*(x)dx = 1.$$

We can image the output fiber wavefront backward onto the SLM plane. The result is a combination of the same lateral Gaussian distribution, with an additional linear phase that depends on fiber output position δ' according to

$$\tan[\theta] = \delta'/f \cong \sin[\theta].$$

Hence, for every output fiber position δ', the corresponding field at the SLM plane is: $\psi_{\rm out}(x) = \psi_{\rm in}(x)\exp[-j\phi(x,\delta')]$, where

$$\phi(x,\delta') = \frac{2\pi}{\lambda}\tan(\theta)x = \frac{2\pi}{\lambda}\frac{\delta'}{f}x. \tag{2}$$

Redirecting the input beam to a specific output fiber port requires a linear phase ramp at the SLM plane

$$\exp[-j\phi(x,\delta)] = \exp\left[-j\frac{2\pi}{\lambda}\frac{\delta}{f}x\right]. \tag{3}$$

This phase ramp will redirect the beam to the output fiber positioned at distance δ from the optical axis.

We should note here that δ' (primed) and δ (not primed) are different in essence: δ denotes the position that the beam is reflected to by the tilting device, whereas δ' denotes any position on the output plane where we want to calculate the coupling. This notation allows us to calculate both the coupling to the chosen output fiber (when $\delta = \delta'$) and the crosstalk in the other output fibers (when $\delta \neq \delta'$). The coupling integral at the SLM plane is given by

$$\eta = \int \psi_{\rm in}(x)\exp[-j\phi(x,\delta)]\psi_{\rm out}^*(x,\delta')dx. \tag{4}$$

In the following, we will calculate the coupling value η in several cases: continuous tilting mirror, pixelated phase deflector, pixelated modulator with phase quantization, and the same modulator with random phase errors. Our model does not include diffraction from the space between pixels (e.g., we assume 100% fill factor), or any interaction between two adjoined pixels (as in *LC*-based phase modulator, where the fringe field affects the sharpness of phase transitions). We also assume infinite SLM extent (no truncation of the beam).

All the reported results of our analysis are analytical expressions, making them more useful as a design tool. We have confirmed these analytical expressions with numerical simulations, which matched perfectly. Since no new information is generated in these simulations, we do not show the simulation results in our figures.

III. Continuous Phase/Mirror

We start with the assumption that the tilted wavefront is achieved with a continuous, infinitely long tilting mirror. The wavefront coming from the fiber on axis is tilted toward a position at distance δ from the optical axis with the phase function in (2). The coupling integral between the output wavefront at δ', and the tilting angle toward δ is

$$\begin{aligned}\eta &= \sqrt{\frac{2}{\pi w_0^2}} \int \exp\left[-\frac{x^2}{w_0^2}\right] \exp\left[j\frac{2\pi}{\lambda}\frac{\delta'}{f}x\right] \\ &\quad \times \exp\left[-j\frac{2\pi}{\lambda}\frac{\delta}{f}x\right] \exp\left[-\frac{x^2}{w_0^2}\right] dx \\ &= \exp\left[-\frac{1}{2}\left(\frac{\delta'-\delta}{w_0'}\right)^2\right].\end{aligned} \tag{5}$$

Hence, the power coupling efficiency is

$$T = |\eta|^2 = \exp\left[-\left(\frac{\delta'-\delta}{w_0'}\right)^2\right] \tag{6}$$

which states that the coupling is dependent on the relative distance between the output and the examined ports. This expected result is shown in Fig. 3. It can be easily seen that for the chosen output fiber $\delta = \delta'$ the overlap integral is unity, as one would expect. To ensure crosstalk level less than 40 dB, the distance between two nearby fibers should satisfy the condition: $\delta - \delta' = \delta_0 \geq 3.035 w_0'$. Fig. 3 shows the fiber coupling efficiency when switching with the mirror to fiber ports -1, 2, and 5.

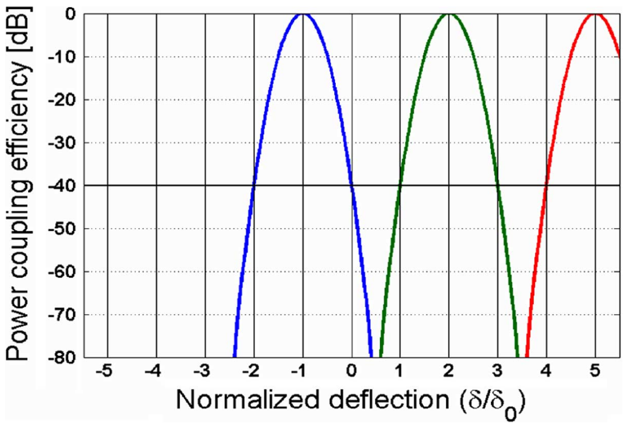

Fig. 3. Fiber coupling efficiency of the switch, set to three different end ports (-1, 2, and 5), in the case of an infinitely long tilting mirror (no pixelization). The distance between fibers is chosen to satisfy 40 dB isolation.

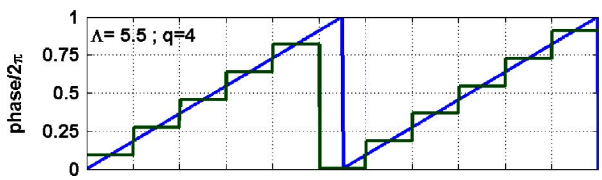

Fig. 4. Graphical depiction of continuous phase (blue) and the sampled phase (green), for $\Lambda = 5.5$.

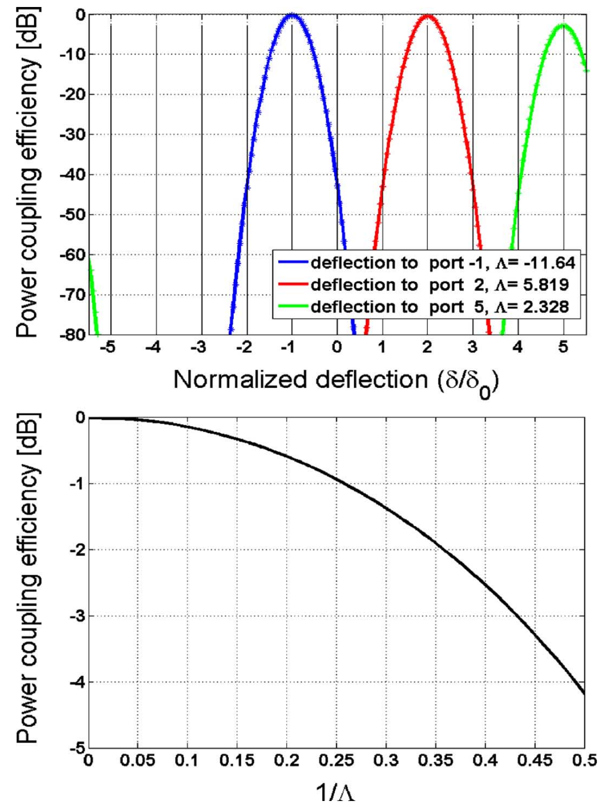

Fig. 5. Top: Fiber coupling efficiency of the switch in the pixelated case ($w_0/p = 18.7$), set to three different end ports ($-1, 2$, and 5). Each deflection angle corresponds to a different value of Λ. The continuous plot is the complete solution ((10)), the "+" and the "x" plot marks the approximations in (11)–(12). Deflection to the fifth port to the right results in residual coupling on the left side since Λ is approaching the limit of $\Lambda = 2$. Bottom: Coupling to the selected fiber as a function of $1/\Lambda$. Large angle tilts imply a decrease in the number of pixels per "saw tooth" and therefore on greater coupling losses.

IV. Pixelization Effect

Replacing the continuous tilting mirror with a pixelated (diffractive), one results in a staircase approximation to the tilted wavefront. The expression for the phase added to the original wavefront in order to deflect it toward the fiber positioned at δ is therefore

$$\begin{aligned}\exp[-j\phi(x,\delta)] &\rightarrow \sum_i \exp[-j\phi(i,\delta)]\ \mathrm{rect}\left[\frac{x-ip}{p}\right]\\ &= \sum_i \exp\left[-j\frac{2\pi}{\lambda}\frac{\delta}{f}x_i\right]\ \mathrm{rect}\left[\frac{x-ip}{p}\right] \quad (7)\end{aligned}$$

where $x_i = ip$ is the central position of the ith pixel of the pixelized SLM (i is running from $-\infty$ to ∞), p is the pixel pitch, and the summation is performed over all the pixels. The pixelized phase SLM operates in modulo 2π mode, as shown in Fig. 4. In order to estimate the quality of the staircase approximation for the tilted wavefront, we introduce the dimensionless parameter Λ, which is equal to the number of pixels in one "saw tooth" period of the applied phase ramp. Since the phase slope is δ/f, as in (3), the number of pixels with pitch size p that will fit in a 2π phase ramp is

$$\Lambda = \frac{\lambda f}{\delta p}. \quad (8)$$

As can be seen in Fig. 4, this value of Λ is not necessarily an integer, but in order to achieve proper deflection, it must be larger than 2, i.e., $\Lambda \geq 2$ (Nyquist sampling criterion).

The diffraction efficiency with the pixelated SLM is

$$\begin{aligned}\eta = \sqrt{\frac{2}{\pi w_0^2}} \int \exp\left[-\frac{x^2}{w_0^2}\right] \exp\left[j\frac{2\pi}{\lambda}\frac{\delta'}{f}x\right]\\ \times \exp\left[-\frac{x^2}{w_0^2}\right] \sum_i \exp\left[-j\frac{2\pi}{\lambda}\frac{\delta}{f}x_i\right] \mathrm{rect}\left[\frac{x-ip}{p}\right] dx. \quad (9)\end{aligned}$$

Rearranging the integration and summation, we find

$$\begin{aligned}\eta = \frac{1}{2}\exp\left[-\frac{1}{2}\left(\frac{\pi w_0 \delta'}{f\lambda}\right)^2\right] \sum_i \exp\left[-j\frac{2\pi}{\lambda}\frac{\delta}{f}x_i\right]\\ \times \left[\mathrm{Erf}\left[\frac{\lambda p(2i+1) - j\pi w_0^2\delta'/f}{\sqrt{2}\lambda w_0}\right]\right.\\ \left. -\mathrm{Erf}\left[\frac{\lambda p(2i-1) - j\pi w_0^2\delta'/f}{\sqrt{2}\lambda w_0}\right]\right]. \quad (10)\end{aligned}$$

This expression is fully analytic and can be evaluated for any fiber position δ'. The value of the error function for a complex argument can be calculated with an algorithm offered in [8].

A reasonable approximation to (10) assumes a relatively small pixel size p, compared to the Gaussian mode w_0. In this case, the Gaussian amplitude is simply sampled at $x_i = ip$, and (9) can be expressed as

$$\begin{aligned}\eta = p\sqrt{\frac{2}{\pi w_0^2}}\mathrm{sinc}\left(\frac{p\delta'}{\lambda f}\right)\\ \times \sum_i \exp\left[-j\frac{2\pi}{\lambda}\frac{\delta-\delta'}{f}ip\right]\exp\left[-\frac{2(ip)^2}{w_0^2}\right] \quad (11)\end{aligned}$$

where we used the definition: $\mathrm{sinc}(x) = \sin(\pi x)/\pi x$.

Equation (11) can be simplified further in the case of a very small pixel size compared to w_0. In that case, the sum can be treated as integral and the coupling equation becomes

$$\eta = \mathrm{sinc}\left(\frac{p\delta'}{\lambda f}\right)\exp\left[-\frac{\pi^2 w_0^2(\delta-\delta')^2}{2(\lambda f)^2}\right]. \quad (12)$$

Fig. 5 shows a comparison between the three results given by (10)--(12), where $w_0/p = 18.7$, and low values of Λ (addressing fiber port positions $-1, 2$, and 5). It can be seen that there is almost no difference in the results as long as the phase is sampled with more than 2 pixels per "saw tooth" period, i.e., $\Lambda \geq 2$.

This simple approximation is especially powerful in showing the dependence of the coupling to the desired fiber as a function of the Λ parameter. Since for $\delta = \delta'$, it becomes

$$\eta(\delta' = \delta) = \mathrm{sinc}\left(\frac{p\delta}{\lambda f}\right) = \mathrm{sin\,c}\left(\frac{1}{\Lambda}\right). \quad (13)$$

This result, as shown in the lower part of Fig. 5, is similar to previous work regarding the diffraction efficiency of a blazing grade [9], [10]. From the earlier results, we can deduce that reducing the number of pixels per period, effects mostly on the coupling to the desired output fiber, but has no effect on the crosstalk to the other fibers. In other words, crosstalk is not caused by the pixelization of the phase. As will be seen in the next sections, this conclusion changes when phase quantization or phase errors are considered.

For notational brevity, the general solution (10) for the coupling integral can be written as

$$\eta(\delta') = A(\delta')\sum_i C_i(\delta')\exp[-j\phi(i,\delta)] \quad (14)$$

where

$$\phi(i,\delta) = 2\pi\frac{p\delta}{\lambda f}i = \frac{2\pi}{\Lambda}i$$

$$A(\delta') = \frac{1}{2}\exp\left[-\frac{1}{2}\left(\frac{\pi w_0\delta'}{f\lambda}\right)^2\right]$$

and

$$C_i(\delta') = \mathrm{Erf}\left[\frac{\lambda p(2i+1) - j\pi w_0^2\delta'/f}{\sqrt{2}\lambda w_0}\right] - \mathrm{Erf}\left[\frac{\lambda p(2i-1) - j\pi w_0^2\delta'/f}{\sqrt{2}\lambda w_0}\right]. \quad (15)$$

And for the approximated solution (11), we use

$$A(\delta') = \sqrt{\frac{2}{\pi}}\frac{p}{w_0}\mathrm{sin\,c}\left(\frac{p\delta'}{\lambda f}\right)$$

$$C_i(\delta') = \exp\left[-\frac{2(ip)^2}{w_0^2} + j\frac{2\pi}{\lambda}\frac{\delta'}{f}ip\right]. \quad (16)$$

In the following, we will regard the solutions we just developed in this compact manner.

V. Phase Quantization Effect

In real, digitally controlled pixelated phase SLM, the actual phase that can be applied is limited by the number of phase levels q. Instead of applying phase of $\phi(i,\delta)$ for the ith pixel, the applied phase values are quantized to discrete levels. Hence, each pixel value is replaced by

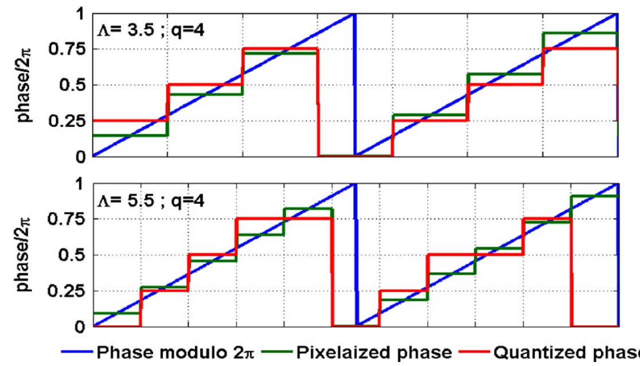

Fig. 6. Graphical depiction of continuous phase (blue), sampled phase (green), and four-level quantized phase (red), for two different Λ values. Larger Λ values represent more samples per phase wrap period.

a quantized phase $\hat{\phi}(i,q,\delta)$, which is the nearest discrete phase level to the desired phase $\phi(i,\delta)$, where $\hat{\phi}(i,q,\delta)$ is defined by

$$\hat{\phi}(i,q,\delta) = \mathrm{Round}\left[\phi(i,\delta)\frac{q}{2\pi}\right]\frac{2\pi}{q} = \mathrm{Round}\left[\frac{q}{\Lambda}i\right]\frac{2\pi}{q}. \quad (17)$$

Fig. 6 demonstrates the effect of pixelization and quantization on the phase applied by the SLM. The analytic solution in (14) is still valid, with a modification of the phase term

$$\eta = A(\delta')\sum_i C_i(\delta')\exp\left[-j\mathrm{Round}\left(\frac{q}{\Lambda}i\right)\frac{2\pi}{q}\right]. \quad (18)$$

The fiber coupling result is shown in Fig. 7—top, for large number of pixels ($\Lambda > 20$) in three deflection cases ($\Lambda = 20.8, \Lambda = 52$, and $\Lambda = 104$), and $q = 103$ discrete phase levels. This quantization case was chosen as it resulted in high crosstalk exactly on a wrong fiber position. The difference from the former results is clear, since the crosstalk level increased dramatically. The red dots on the plot denote the maximum crosstalk level (for nonadjacent ports). There is no simple relationship between the number of pixels per period Λ, the quantization levels q, and the maximal crosstalk. However, high crosstalk levels occur whenever the ratio q/Λ is close to being an integer, as the summation term of the $\mathrm{round}(\cdot)$ function over i will exhibit few discontinuous phase jumps. When the ratio q/Λ is far from being an integer, there will be many discontinuous phase jumps, which dephase the coupling to other fibers and lower the crosstalk. In the special case, as shown in Fig. 7, we observe high crosstalk values on other ports when the chosen output port is $5(\mathrm{q}/\Lambda = 103/20.8 = 4.95), 3(\mathrm{q}/\Lambda = 103/52 = 1.98)$, or $-1(\mathrm{q}/\Lambda = 103/104 = 0.99)$); there is no direct way to predict on which neighboring fiber the highest crosstalk will be observed. In Fig. 8 (bottom), the crosstalk values as a function of quantization levels divided by the pixel count per period (using $\Lambda = 20.8$) are shown, where the calculation was made for three different definitions: crosstalk average, average plus one standard deviation (STD), and worst case levels. Again, we observe elevated crosstalk levels whenever q/Λ is close to being an integer value. When q/Λ is exactly an integer, there is no crosstalk (the sampled values depicted in the graph sometimes miss these occurrences). The crosstalk levels decrease with increasing phase quantization values, as the discontinuous phase jumps are smaller in magnitude and diffract less light to undesired directions. Crosstalk can be suppressed to less than -40 dB for $q > 100$ levels.

Returning to the diffraction efficiency calculation [see Fig. 7 (bottom)], one can see that for large number of phase levels

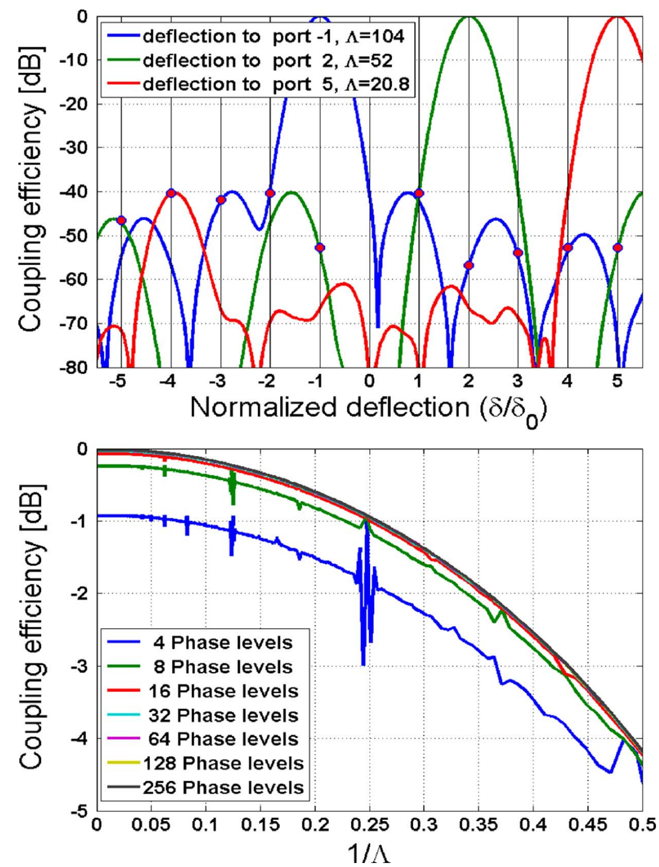

Fig. 7. Top: Fiber coupling efficiency of the switch with quantized phase ($q = 103$), set to three different end ports (-1, 2, and 5). The red dots denote maximum crosstalk level (for nonadjacent ports). Bottom: Coupling to the selected fiber as a function of $1/\Lambda$ and quantization phase levels. It is easy to see that for small number of phase levels the singular points that obey the condition $q/\Lambda = \mathrm{integer}$ give much better results. However, for phase levels higher than 16, the insertion loss converges to the graph determined solely by Λ as in Fig. 5.

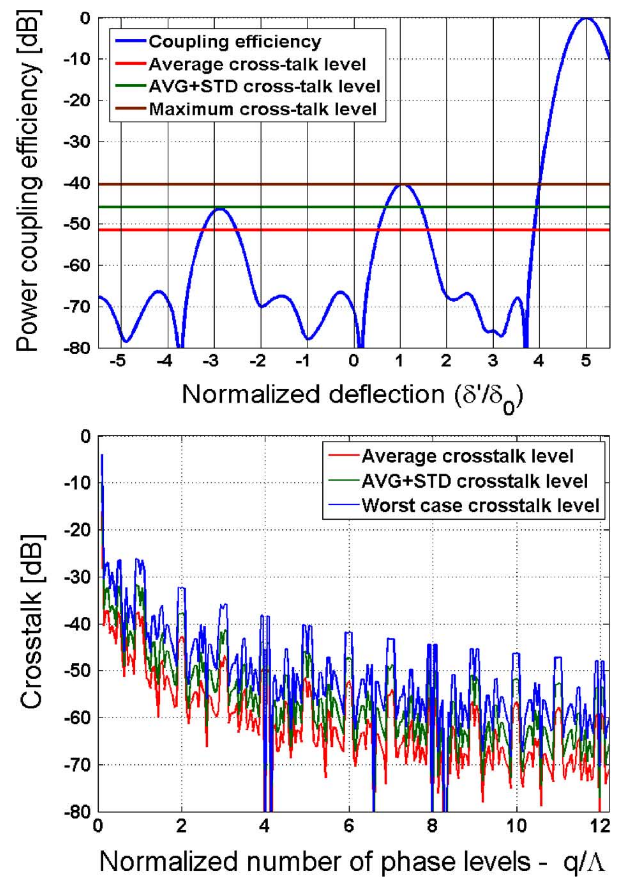

Fig. 8. Top: Fiber coupling efficiency of the switch, set to port 5, with 103-level phase quantization. Crosstalk average, average + one standard deviation, and worse case levels shown. Bottom: Observed crosstalk levels as a function of quantization values divided by the number of pixels per period. High crosstalk levels occurs when the ratio q/Λ is close to being an integer, but disappear when it is an integer. Crosstalk levels can be significantly suppressed only for $q > 100$ levels.

$(\mathrm{q} > 16)$, the phase quantization effect on the power coupling loss is almost negligible. Even for $q < 16$, whenever $q/\Lambda =$ integer, the value of the quantized phase is equal to the actual phase since

$$\mathrm{Round}\left(\frac{q}{\Lambda}i\right)\frac{2\pi}{q} = \frac{2\pi}{\Lambda}i.$$

Allegedly, we can attempt to design the distance between fibers δ_0 such that q/Λ is an integer (or $q\delta_0 p/\lambda f = N$, where N is an integer). In this case, the performance reverts back to the sampled (pixelized) case, resulting in coupling dependent on Λ (see Fig. 5) and no crosstalk. However, since any little error in the fiber position or support of multiple wavelengths will result in a noninteger value for q/Λ, other considerations must be made as a noninteger value will result in higher crosstalk levels. We consider two reasonable schemes for crosstalk reduction. The first is to use a high number of phase quantization levels. Our results show that with more than 100 phase levels the crosstalk produced is low. This can be explained by the discontinuous phase jumps due to the rounding operation being of small magnitude and not being able to significantly redirect energy. The second, more radical way is to operate with a relatively small number of phase levels but with q/Λ values far from integers. The coupling efficiency result will be slightly worse, but lower crosstalk can be easily achieved, due to the dephasing effect.

VI. Random Phase Error Effect

In addition to the phase quantization, the actual phase applied by the SLM may suffer from fluctuations, resulting in random phase errors. To consider phase errors effect, we follow the work of [11] on fabrication errors in arrayed waveguide gratings, and apply it to our problem. Our analysis starts by determining that the error of the pixel phase is combined from the desired phase value $\phi(x_i)$ and a phase error: $\delta\phi(x_i)$. This leads to the expression

$$\eta = A(\delta')\sum_i C_i(\delta')\exp[j[\phi(x_i) + \delta\phi(x_i)]] \tag{19}$$

where $\delta\phi(x_i)$ is the phase error of the SLM ith pixel. Since the interesting value is the power coupling efficiency, we should calculate the statistics of $T = |\eta|^2$ instead of η. We are interested in the mean value of the crosstalk $\langle T\rangle$ for the expected level of performance but also in the standard deviation (STD) of the crosstalk, to ensure a 40 dB crosstalk-proof system.

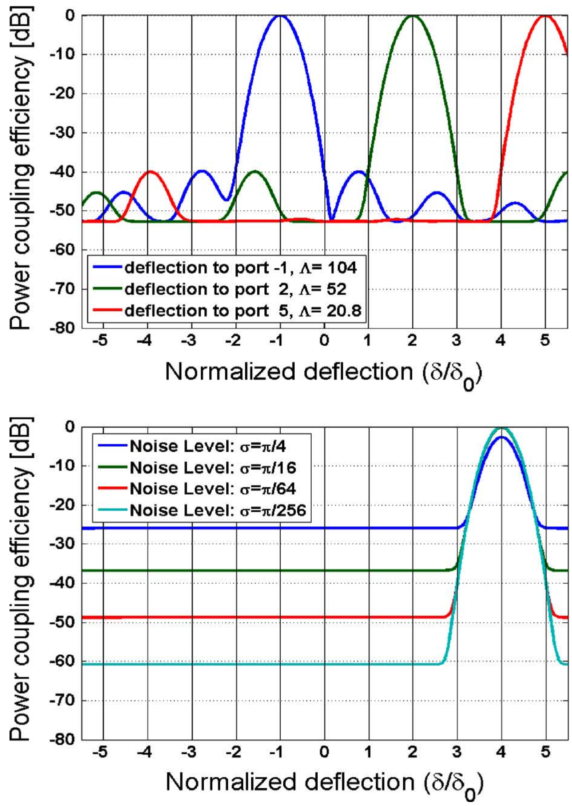

Fig. 9. Top: Fiber coupling efficiency of the switch with quantization and random phase errors, set to three different ports (-1, 2, and 5), where $q = 102$ and with the addition of Gaussian noise assuming $\sigma = (2\pi/q)/2$ (half phase level). Bottom: Fiber coupling efficiency of the switch with random phase error only, $\Lambda = 20.8$. Switch set to fourth port with four noise levels: $\sigma = p/4, p/16, p/64$, and $p/256$.

The mean value of the power coupling efficiency is provided by the expression (for convenience we omit the δ' from the notation of A and C_i, and denote $\delta\phi(x_i)$ as δ_i).

$$\begin{aligned}\langle T\rangle &= \langle|\eta|^2\rangle = \left\langle\left|A\sum_i C_i\exp[j\phi(x_i)]\exp[j\delta_i]\right|^2\right\rangle\\ &= \left\langle A^2\sum_i\sum_k C_iC_k\exp\left[j\phi\left(x_i\right)\right]\right.\\ &\qquad \left.\times\exp[j\delta_i]\exp[-j\phi(x_k)]\exp[-j\delta_k]\right\rangle\\ &= A^2\sum_i\sum_k C_iC_k\exp[j[\phi(x_i)-\phi(x_k)]]\\ &\qquad\times\langle\exp[j[\delta_i-\delta_k]]\rangle. \end{aligned}\tag{20}$$

Assuming that δ_i is an independent random variable yields

$$\langle\exp[j[\delta\phi_i-\delta\phi_k]]\rangle = \begin{cases}\langle\exp[j\delta_i]\rangle\langle\exp[-j\delta_k]\rangle & i\neq k\\ 1 & i=k\end{cases}. \tag{21}$$

We further assume an identically distributed Gaussian distribution for δ_i, with a zero average error, and variance of $\langle\delta_i^2\rangle = \sigma^2$. The expectation value of the phase exponent is hence

$$\langle\exp[j\delta_i]\rangle = \exp[-\sigma^2/2]. \tag{22}$$

Substitution of the result yields the expression for $\langle T\rangle$ and after some manipulations, we get

$$\begin{aligned}\langle T\rangle = \exp(-\sigma^2)&\left|A\sum_i C_i\exp[j[\phi(x_i)]]\right|^2\\ &+A^2(1-\exp(-\sigma^2))\sum_i C_i^2. \end{aligned}\tag{23}$$

Using the fact that the power coupling without phase errors is described by

$$T_{\mathrm{error-free}} \equiv \left|A\sum_i C_i\exp[j[\phi(x_i)]]\right|^2. \tag{24}$$

We conclude with the relatively simple expression

$$\langle T\rangle = \exp(-\sigma^2)T_{\mathrm{error-free}} + A^2(1-\exp(-\sigma^2))\sum_i C_i^2. \tag{25}$$

While the first term is dominant in when $\delta = \delta'$ ($T_{\mathrm{error-free}}$ is then equal to unity), the second is dominant when $\delta \neq \delta'$ and will affect the crosstalk.

In Fig. 9(bottom), the effect of the random phase error is shown for the case of unquantized phase SLM with random phase error only. It can be seen that as σ gets bigger, the coupling efficiency for the selected output fiber is decreasing while the crosstalk level is increasing. In the quantized case, σ will not be more than half of a phase level, so the primary impact of the phase error is on the crosstalk level.

In Fig. 9(Top), the random phase error is added to the same condition that was presented in Fig. 7(Top). Since $\sigma = (2\pi/\mathrm{q})/2$, the effect on the coupling is negligible, but the crosstalk floor is higher.

While the calculation of the expected value of T was relatively short, the calculation of its STD is quite tedious. A rigorous calculation of the STD is outlined in the Appendix. In general, its calculation requires the evaluation of $\langle T^2\rangle$, since $\mathrm{STD}^2(T) = \langle T^2\rangle - \langle T\rangle^2$. The result is an average on all the possible combinations of the four phase errors: $\langle\exp[j[\delta_i-\delta_k+\delta_l-\delta_m]]\rangle$. Since for different values of i, k, l, and m the average on the exponent will differ, one must calculate the average for each case separately (as shown in the Appendix). With this approach, after some manipulations, we get the approximate simple expression

$$\mathrm{STD}^2(T) \cong \langle T\rangle^2 - \exp[-2\sigma^2]T^2_{\mathrm{error-free}} \tag{26}$$

where $T_{\mathrm{error-free}}$ is defined by (24).

Since $\sigma \ll 1$ the result is approximately equal to

$$\mathrm{STD}^2(T) \cong \langle T\rangle^2 - T^2_{\mathrm{ErrorFree}} \tag{27}$$

which makes sense because near the peak $\langle T\rangle^2 \cong T^2_{\mathrm{ErrorFree}}$ and therefore the $\mathrm{STD}(T)$ is small. On the other hand, far away from the peak (in the crosstalk region), $\langle T\rangle^2 \gg T^2_{\mathrm{ErrorFree}}$, and then $\mathrm{STD}(T) \cong \langle T\rangle$. The addition of the power coupling STD is shown in Fig. 10. It can be seen that for the same parameters, as shown in Fig. 9(Top) (switching toward the fifth port), the crosstalk calculated with the phase error consideration is now at risk of being more than -40 dB at 1 STD level of confidence. This implies that the crosstalk level is highly dependent on low phase noise of the SLM.

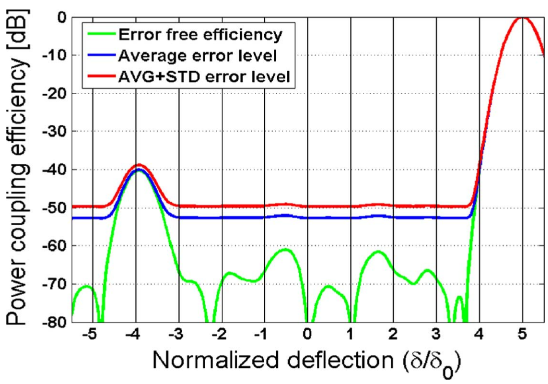

Fig. 10. Fiber coupling efficiency of the switch with phase pixelization and quantization and with the addition of random phase error. Switch set to fifth port with $q = 102, \Lambda = 20.84$, we assume Gaussian noise with $\sigma = (2\pi/q)/2$ (half phase level).

VII. Conclusion and Summary

We have found that a few basic parameters influence the switching characteristics when using pixelized SLM instead of a continuous mirror. The pixel size impacts the increasing coupling losses for fibers that require large tilting angles, due to sampling of the phase function. The phase quantization levels give rise to random errors and scattering off the array, manifest as crosstalk on neighboring fibers. The crosstalk increases for fewer phase quantization levels. Random phase errors contribute mostly to the crosstalk level. These findings imply that for satisfying performance of such a system, one has to use phase SLM with as many as possible pixels and phase levels, and with low phase noise.

As we emphasized earlier, it is possible theoretically to find the exact arrangement (e.g., the distance between fibers, lens focal length, pixel size, and wavelength) in which q/Λ is an integer. The performance under this situation will be much better, since the quantized phase is equal to the case of unquantized phase. Therefore, even with small number of phase levels, we will get good results as long as we keep the phase noise small enough.

However, this arrangement will be affected strongly by errors in the fiber positions and will not support broadband light (as in the case of wavelenght-division multiplexing), as these cases will result in noninteger values for q/Λ. To overcome this, one may choose from two reasonable possibilities: using a high number of phase levels, or choose a far-from-integer relation for q/Λ.

Nevertheless, the importance of the aforementioned calculations is in the ability to forecast the power coupling and the crosstalk in system with the given parameters-pixel size, phase levels, and phase error.

A last point to note is that additional effects, that were not discussed here, impact real devices. LCOS SLM will suffer mostly from the fringe field effect between pixels, where MEMS modulator will have lower fill factor, which will reduce the diffraction efficiency.

Appendix
Power Coupling STD Calculations

In this appendix, we evaluate $\langle T^2\rangle$, in order to find the standard deviation that equals to: $\mathrm{STD}(T) = \langle T^2\rangle - \langle T\rangle^2$.

For brevity, we define: $D_i = A(\delta')C_i(\delta')\exp[j\phi(x_i)]$. Hence,

$$\eta = \sum_i D_i \exp[j\delta\phi(x_i)]. \tag{28}$$

And the power coupling efficiency will be

$$T = |\eta|^2 = \sum_{i,k} D_i D_k^* \exp[j(\delta\phi(x_i) - \delta\phi(x_k))]. \tag{29}$$

Using this notation to describe $\langle T\rangle$ and $T_{\text{error-free}}$ yields

$$T_{\text{error-free}}(\delta') = \left|\sum_i D_i(\delta')\right|^2 = \sum_i\sum_k D_i D_k^* \tag{30}$$

$$\langle T\rangle = \exp(-\sigma^2)T_{\text{error-free}} + \sum_i |D_i|^2(1-\exp(-\sigma^2)). \tag{31}$$

A. Calculating the Expectation Value of T^2

Substituting (29) in the expectation value of $\langle T^2\rangle$ leads to

$$\begin{aligned}\langle T^2\rangle &= \langle|\eta|^2|\eta|^2\rangle \\ &= \left\langle \left|\sum_i D_i\exp[j\delta_i]\right|^2 \left|\sum_l D_l\exp[j\delta_l]\right|^2\right\rangle \\ &= \sum_i\sum_k\sum_l\sum_m D_iD_k^*D_lD_m^*\langle\exp[j[\delta_i-\delta_k+\delta_l-\delta_m]]\rangle.\end{aligned} \tag{32}$$

In order to calculate the expectation value of $\langle\exp[j[\delta_i-\delta_k+\delta_l-\delta_m]]\rangle$, we should consider the different possible combinations of: i, k, l, and m, taking into account that δ_i is an independent, identically distributed Gaussian random variable. There are 15 different combinations of the indices, depending whether the indexes are equal or not.
We demonstrate one case for an example:
For $i \neq k, i \neq l, i \neq m$, we get

$$\begin{aligned}&\langle\exp[j[\delta_i-\delta_k+\delta_l-\delta_m]]\rangle \\ &\quad = \langle\exp[j\delta_i]\rangle\langle\exp[j[-\delta_k+\delta_l-\delta_m]]\rangle.\end{aligned} \tag{33}$$

In this case, for $k \neq l, k \neq m$ we get

$$= \langle\exp[j\delta_i]\rangle\langle\exp[-j\delta_k]\rangle\langle\exp[j[\delta_l-\delta_m]]\rangle. \tag{34}$$

Now, if $l = m$, the expectation value of the phase difference term is unity; hence, we have

$$= \begin{cases}\langle\exp[j\delta_i]\rangle\langle\exp[-j\delta_k]\rangle\langle\exp[j\delta_l]\rangle\langle\exp[-j\delta_m]\rangle & l\neq m \\ \langle\exp[j\delta_i]\rangle\langle\exp[-j\delta_k]\rangle & l = m\end{cases}. \tag{35}$$

In the same manner and with substitution of the result from (22) , we get 15 different combinations that are defined by the following terms:

$$\begin{aligned}\exp[-4\sigma^2] &\leftrightarrow i = l \neq k = m \\ \exp[-3\sigma^2] &\leftrightarrow \begin{cases} i\neq l\neq k = m \\ i = l\neq k\neq m\end{cases} \\ \exp[-2\sigma^2] &\leftrightarrow i\neq l\neq k\neq m \\ 1 &\leftrightarrow \begin{cases} i = k\neq l = m \\ i = m\neq k = l \\ i = l = k = m\end{cases} \\ \exp[-\sigma^2] &\leftrightarrow \text{otherwise}.\end{aligned} \tag{36}$$

$$
\begin{aligned}
\langle T^2\rangle &= 2\sum_{i,k}|D_i|^2|D_k|^2 - \sum_i |D_i|^4 \\
&\quad + \exp[-\sigma^2]\begin{pmatrix} -4\sum_{i,k}|D_k|^2|D_l|^2 + 4\sum_i |D_i|^4 \\ +4\sum_{i,k,l} D_iD_k^*|D_l|^2 - 2\sum_{i,k} D_iD_k^*|D_k|^2 - 2\sum_{i,k} D_iD_k^*|D_i|^2 \end{pmatrix} \\
&\quad + \exp[-2\sigma^2]\begin{pmatrix} \sum_i\sum_k\sum_l\sum_m D_iD_k^*D_lD_m^* - 4\sum_{i,k,l} D_iD_k^*|D_l|^2 \\ -\sum_{i,k,l} D_iD_l(D_k^*)^2 - \sum_{i,k,l}(D_i)^2D_k^*D_l^* + 4\sum_{i,k} D_iD_k^*|D_k|^2 \\ 4\sum_{i,k} D_iD_k^*|D_i|^2 + 2\sum_{i,k}|D_i|^2|D_k|^2 + \sum_{i,k}(D_i)^2(D_k^*)^2 - 6\sum_i |D_i|^4 \end{pmatrix} \\
&\quad + \exp[-3\sigma^2]\begin{pmatrix} \sum_{i,k,l} D_iD_l(D_k^*)^2 + \sum_{i,k,l}(D_i)^2D_k^*D_l^* - 2\sum_{i,k} D_iD_k^*|D_i|^2 \\ -2\sum_{i,k} D_iD_k^*|D_k|^2 - 2\sum_{i,k}(D_i)^2(D_k^*)^2 + 4\sum_i |D_i|^4 \end{pmatrix} \\
&\quad + \exp\left[-4\sigma^2\right]\left(\sum_{i,k}(D_iD_k^*)^2 - \sum_i |D_i|^4\right)
\end{aligned} \tag{39}
$$

$$
\begin{aligned}
\mathrm{STD}^2(T) &= \langle T^2\rangle - \langle T\rangle^2 = \langle T\rangle^2 - \sum_i |D_i|^4 \\
&\quad + \exp[-\sigma^2]\left(-2\sum_{i,k} D_iD_k^*|D_k|^2 - 2\sum_{i,k} D_iD_k^*|D_i|^2 + 4\sum_i |D_i|^4\right) \\
&\quad + \exp[-2\sigma^2]\begin{pmatrix} -\sum_i\sum_k\sum_l\sum_m D_iD_k^*D_lD_m^* - \sum_{i,k,l} D_iD_l(D_k^*)^2 \\ -\sum_{i,k,l}(D_i)^2D_k^*D_l^* + 4\sum_{i,k} D_iD_k^*|D_k|^2 \\ 4\sum_{i,k} D_iD_k^*|D_i|^2 + \sum_{i,k}(D_i)^2(D_k^*)^2 - 6\sum_i |D_i|^4 \end{pmatrix} \\
&\quad + \exp[-3\sigma^2]\begin{pmatrix} \sum_{i,k,l} D_iD_l(D_k^*)^2 + \sum_{i,k,l}(D_i)^2D_k^*D_l^* - 2\sum_{i,k} D_iD_k^*|D_i|^2 \\ -2\sum_{i,k} D_iD_k^*|D_k|^2 - 2\sum_{i,k}(D_i)^2(D_k^*)^2 + 4\sum_i |D_i|^4 \end{pmatrix} \\
&\quad + \exp[-4\sigma^2]\left(\sum_{i,k}(D_iD_k^*)^2 - \sum_i |D_i|^4\right)
\end{aligned} \tag{40}
$$

Substitution of the results in the sum and combining similar terms, we will get the following expression:

$$
\begin{aligned}
\langle T^2\rangle &= \sum_i\sum_k\sum_l\sum_m D_iD_k^*D_lD_m^*\langle\exp[j[\delta_i-\delta_k+\delta_l-\delta_m]]\rangle \\
&= \sum_{i\neq k\neq l\neq m} D_iD_k^*D_lD_m^*\exp[-2\sigma^2] + 4\sum_{i\neq k\neq l} D_iD_k^*|D_l|^2\exp[-\sigma^2] \\
&\quad + 2\sum_{i\neq k} D_iD_k^*|D_k|^2\exp[-\sigma^2] + 2\sum_{i\neq k} D_iD_k^*|D_i|^2\exp[-\sigma^2] \\
&\quad + \sum_{i\neq k\neq l} D_iD_l(D_k^*)^2\exp[-3\sigma^2 + \sum_{i\neq k\neq l}(D_i)^2D_k^*D_l^*\exp[-3\sigma^2] \\
&\quad + \sum_{i\neq k}(D_iD_k^*)^2\exp[-4\sigma^2] + 2\sum_{i\neq k}|D_i|^2|D_k|^2 + \sum_i |D_i|^4.
\end{aligned} \tag{37}
$$

B. Rewriting the Expression as Sum of Complete Series

In order to calculate $\langle T^2\rangle$ explicitly, we should replace the partial sums in (37) with a sum of complete series. As an example, the expression $\sum_{i\neq k}|D_i|^2|D_k|^2$ will be written now as

$$\sum_{i\neq k}|D_i|^2|D_k|^2 = \sum_{i,k}|D_i|^2|D_k|^2 - \sum_i |D_i|^4. \tag{38}$$

Using the same method for the rest of the expressions, (37) will now take the form shown in (39) at the top of the page.

C. Calculating $\langle T^2\rangle - \langle T\rangle^2$

Taking the square of $\langle T\rangle$ (31) and subtracting from (39) yields (40), shown at the top of the page.

D. Simple Approximation of the Results

Careful examination of (40) shows that the term $\sum_i \sum_k \sum_l \sum_m D_i D_k^* D_l D_m^*$ is much more dominant than the others, since only this term does not involve higher powers of D_i. Moreover, all the other terms cancel each other when assuming $\sigma \ll 1$. Equation (40) , therefore, can be reduced to

$$\mathrm{STD}^2(T) \cong \langle T \rangle^2 - \exp[-2\sigma^2] T^2_{\mathrm{error-free}} \tag{41}$$

where we used the equality

$$T^2_{\mathrm{error-free}} \equiv \sum_i \sum_k \sum_l \sum_m D_i D_k^* D_l D_m^*. \tag{42}$$

REFERENCES

[1] Y.-A. Peter, F. Gonté, H. P. Herzig, and R. Dändliker, "Micro-optical fiber switch for a large number of interconnects using a deformable mirror ," *IEEE Photon. Technol. Lett.*, vol. 14, no. 3, pp. 301–303, Mar. 2002.

[2] D. M. Marom, D. T. Neilson, D. S. Greywall, C. S. Pai, N. R. Basavanhally, V. A. Aksyuk, D. O. López, F. Pardo, M. E. Simon, Y. Low, P. Kolodner, and C. A. Bolle, "Wavelength-selective $1 \times K$ switches using free-space optics and MEMS micromirrors: Theory, design, and implementation," *IEEE J. Lightw. Technol.*, vol. 23, no. 4, pp. 1620–30, Apr. 2005.

[3] H. R. Shea, S. Arney, A. Gasparyan, M. Haueis, V. A. Aksyuk, C. A. Bolle, R. E. Frahm, S. Goyal, F. Pardo, and M. E. Simon, "Design for reliability of MEMS/MOEMS for lightwave telecommunications," in *Proc. Lasers Electro-Opt. Soc. 2002*, vol. 1, pp. 418–419.

[4] P. F. McManamon, P. J. Bos, M. J. Escuti, J. Heikenfeld, S. Serati, X. Huikai, and E. A. Watson, "A review of phased array steering for narrowband electrooptical systems," *Proc. IEEE*, vol. 97, no. 6, pp. 1078–1096, Jun. 2009.

[5] G. Baxter, S. Frisken, D. Abakoumov, H. Zhou, I. Clarke, A. Bartos, and S. Poole, "Highly programmable wavelength selective switch based on liquid crystal on silicon switching elements ," presented at the Optical Fiber Communication, Eveleigh, NSW, 2006.

[6] I. W. Jung, J. S. Wang, and O. Solgaard, "Optical pattern generation using a spatial light modulator for maskless lithography," *IEEE J. Sel. Topics Quantum Electron.*, vol. 13, no. 2, pp. 147–154, Mar./Apr. 2007.

[7] B. Apter, U. Efron, and E. Bahat-Treidel, "On the fringing-field effect in liquid-crystal beam-steering devices," *Appl. Opt.*, vol. 43, no. 1, pp. 11–19, Jan. 2004.

[8] J. A. C. Weideman, "Computation of the complex error function," *SIAM J. Numer. Anal.*, vol. 31, pp. 1497–1518, Oct. 1994.

[9] Tan *et al.*, "Dynamic holography for optical interconnections. II. Routing holograms with predictable location and intensity of each diffraction order," *J. Opt. Soc. Amer. A*, vol. 18, pp. 205–215, 2001.

[10] E. Hallstig, L. Sjoqvist, and M. Lindgren, "Intensity variations using a quantized spatial light modulator for nonmechanical beam steering ," *Opt. Eng.*, vol. 42, pp. 613–619, 2003.

[11] T. Kamalakis, T. Sphicopoulos, and D. Syvridis, "An estimation of performance degradation due to fabrication errors in AWGs," *J. Lightw. Technol.*, vol. 20, no. 9, pp. 1779–1787, Sep. 2002.

David Sinefeld, biography not available at the time of publication.

Dan M. Marom (M'00–SM'07) received the B.Sc. degree in mechanical engineering and the M.Sc. degree in electrical engineering, both from Tel-Aviv University, Tel-Aviv, Israel, in 1989 and 1995, respectively, and the Ph.D. from the University of California, San Diego (UCSD), in 2000.

In his doctoral dissertation he investigated femtosecond-rate optical signal processing with applications in ultrafast communications. From 1996 through 2000, he was a Fannie and John Hertz Foundation Graduate Fellow at UCSD. From 2000 until 2005, he was a Member of the Technical Staff at the Advanced Photonics Research Department at Bell Laboratories, Lucent Technologies, where he worked on novel MEMS based switching solutions using MEMS technology for optical communications. Since 2005, he has been with the Applied Physics Department, Hebrew University, where he is pursuing his research interests in creating photonic devices for switching and manipulating optical signals, using light modulating devices, nonlinear optics, and compound materials.

Dr. Marom was a Peter Brojde Scholar in 2006-2007.